STEM CELLS AND DEVELOPMENT
Volume 30, Number 23, 2021

DOI: 10.1089/scd.2021.0124

Histology Scoring System for Murine Cutaneous Wounds

Mari van de Vyver,[1] Kiara Boodhoo,[1] Trivia Frazier,[2,i] Katie Hamel,[2] Marta Kopcewicz,[3] Benjamin Levi,[4] Michelle Maartens,[1] Sylwia Machcinska,[3] Johanna Nunez,[4] Chase Pagani,[4] Emma Rogers,[2] Katarzyna Walendzik,[3] Joanna Wisniewska,[3] Barbara Gawronska-Kozak,[3] and Jeffrey M. Gimble[2,5]

Monitoring wound progression over time is a critical aspect for studies focused on in-depth molecular analysis or on evaluating the efficacy of potential novel therapies. Histopathological analysis of wound biopsies can provide significant insight into healing dynamics, yet there is no standardized and reproducible scoring system currently available. The purpose of this study was to develop and statistically validate a scoring system based on parameters in each phase of healing that can be easily and accurately assessed using either Hematoxylin & Eosin (H&E) or Masson's Trichrome (MT) staining. These parameters included re-epithelization, epithelial thickness index, keratinization, granulation tissue thickness, remodeling, and the scar elevation index. The initial phase of the study was to (1) optimize and clarify healing parameters to limit investigator bias and variability; (2) compare the consistency of parameters assessed using H&E versus MT staining. During the validation phase of this study, the accuracy and reproducibility of this scoring system was independently iterated upon and validated in four different types of murine skin wound models (Excisional; punch biopsy; pressure ulcers; burn wounds). A total of $n = 54$ histology sections were randomized, blinded, and assigned to two groups of independent investigators ($n = 5$ per group) for analysis. The sensitivity of each parameter (ranging between 80% and 95%) is reported with illustrations on the appropriate assessment method using ImageJ software. In the validated scoring system, the lowest score (score:0) is associated with an open/unhealed wound as is evident immediately and within the first day postinjury, whereas the highest score (score:12) is associated with a completely closed and healed wound without excessive scarring. This study defines and describes the minimum recommended criteria for assessing wound healing dynamics using the SPOT skin wound score. The acronym SPOT refers to the academic and scientific institutions that were involved in the development of the scoring system, namely, Stellenbosch University, Polish Academy of Sciences, Obatala Sciences, and the University of Texas Southwestern.

Keywords: pressure ulcer, diabetic ulcer, excisional wounds, wound healing, wound scoring

Introduction

Over the last two decades (2000–2018), chronic wounds with mixed etiologies were estimated to affect 2.21 per 1,000 population globally [1]. These wounds can be divided into three classes: pressure ulcers/injuries (prolonged bed rest/ICU patients), ischemic leg ulcers (microvascular disease), and diabetic foot ulcers (uncontrolled hyperglycemia) [2]. In 2018, a retrospective analysis in the United States indicated that wound care costs range between US$28–96 billion annually, with the highest expense associated with outpatient care due to the lack of efficient or effective treatment strategies [3]. The recurrence rate of chronic wounds can be as high as 20%–80% especially in the case of diabetic ulcers [4]. Since underlying conditions such as age, stress, obesity, and diabetes (DM) are associated with dysfunctional healing responses, the prevalence of chronic wounds are expected to increase considerably in the near future [5]. In addition to placing enormous strain on health care systems, chronic wounds can have debilitating consequences for patients [1,3,5,6].

[1]Division of Clinical Pharmacology, Department of Medicine, Faculty of Medicine and Health Sciences, Stellenbosch University, Cape Town, South Africa.
[2]Obatala Sciences, Inc., New Orleans, Louisiana, USA.
[3]Institute of Animal Reproduction and Food Research, Polish Academy of Sciences, Olsztyn, Poland.
[4]Department of Surgery, University of Texas Southwestern Medical Center, Dallas, Texas, USA.
[5]Department of Medicine, Structural and Cellular Biology, and Surgery, Center for Stem Cell Research and Regenerative Medicine, Tulane University School of Medicine, New Orleans, Louisiana, USA.
[i]ORCID ID (https://orcid.org/0000-0003-1689-0987).

Monitoring wound progression over time is a critical aspect for studies focused on in-depth molecular analysis or on evaluating the efficacy of potential novel therapies. Histopathological analysis of wound biopsies can provide significant insight into healing dynamics, yet there is no standardized and reproducible scoring system currently available. Wound healing is a complex and highly regulated process that involves the progression through four distinct yet overlapping phases namely, hemostasis (blood clotting scab formation), inflammation (immune response/phagocytosis), proliferation (cellular mediators of repair), and remodeling (restoration of function) [7]. Disruption or dysregulation as the result of either underlying pathology or external factors can occur at any of these stages. Chronic wounds are often associated with a prolonged and excessive inflammatory response and fail to progress into the proliferative stage of healing [8]. Furthermore, in the case of burn wounds, hypertrophic scarring that severely affects tissue function is often evident [9]. Both chronic wounds and burn wounds are prone to necrotizing skin and soft tissue infections [10]. There is thus a need for extensive studies using animal models to investigate the underlying biological mechanisms associated with dysfunctional healing responses to improve treatment outcomes in patients with chronic wounds [2,5].

The purpose of this study was to develop and validate a histology scoring system based on the different parameters in each phase of healing that can be easily and accurately assessed using either Hematoxylin & Eosin (H&E) or Masson's Trichrome (MT) staining. The accuracy and reproducibility of this scoring system was independently iterated upon and validated in four different types of murine skin wound models.

Materials and Methods

This was an international collaborative study with investigators from four institutions namely, Stellenbosch University (South Africa), Polish Academy of Sciences in Olsztyn (Poland), University of Texas Southwestern Medical Center (Texas, USA), and Obatala Sciences, Inc., (New Orleans, LA). Each research group contributed archived H&E and MT-stained tissue sections derived from a variety of murine skin wound models. All archived tissue sections were derived from studies with Institutional Animal Care and Use approval (SU-ACUD17-000016 Stellenbosch University; IACUC Protocol 772, approval date December 2, 2020 Tulane University; No. 22/2015 University of Warmia and Mazury), no additional animals were wounded for the sole purpose of this study. These studies complied with the South African Animal Protection Act (Act no 71, 1962), the American Veterinary Medical Association (AVMA) guidelines. All experiments were conducted according to the ethical guidelines and principles of the declaration of Helsinki.

Murine wound models

Model 1. Excisional: healthy control versus obese Type 2 diabetes (DM). Two identical bilateral dorsal full-thickness excisional wounds were made on male obese type 2 DM mice (B6.Cg-lep^{ob}/J, ob/ob) (10–12 weeks old) with blood glucose levels >300 mg/dL. This chronic wound model was optimized to more closely mimic the clinical setting by injecting neutral endopeptidase (NEP) (1.02 mg/μL; 150 pmol/h/μg) (SRP6450, Neprilysin/CD10; Sigma-Aldrich) subcutaneously around the wound edges as previously described [8]. As parallel control acute wounds were induced using the same procedure on healthy wild-type (WT) control mice (C57BL/6J) (10–12 weeks old; blood glucose <200 mg/dL). The animals were housed individually for a period of 7 days postinjury with free access to food and drinking water before euthanasia and harvesting of the wound tissue for processing and subsequent histological analysis. Paired H&E and MT-stained sections from this model was included for the optimization ($n=10$ WT control) and validation ($n=3$ WT control; $n=4$ obese DM) phase of this study.

Model 2. Punch biopsy: aging and obesity. Four full-thickness excisional wounds (4 mm biopsy punch, Miltex) were created on the back of young (2–3 months) and old (16–18 months) wild-type (WT) mice (C57BL/6J) that had been fed either a low-fat diet (LFD, 13 kcal% fat; PicoLab Rodent Diet 20 5053) or high fat diet (HFD 59 kcal% fat; TestDiet AIN-76A; LabDiet) for a period of 8 weeks as previously described [11]. Postinjury skin tissues were collected with 8 mm diameter biopsy punches after euthanasia on days 3,7,14, and 21 postwounding and processed for subsequent histological staining and analysis. H&E ($n=7$) and MT-stained ($n=9$) sections derived from this model ($n=6$ young, $n=10$ old) were included in the validation phase of the study.

Model 3. Pressure ulcer: Healthy control versus delayed healing. Bilateral symmetric dorsal pressure ulcers were formed by placing a dorsal skin fold between two circular magnets for two complete ischemia (12 h) -reperfusion (12 h) (IR) 24 h cycles using female 8-week-old C57BL/6 mice as previously described [12]. Immediately after induction of the IR injury, 0.15 μg NEP (in a volume of 30 μL of sterile PBS) was injected subcutaneously at each wound site to model the delayed healing state. The healthy control grouping was left without any further manipulation after IR injury. Mice were maintained for 14 days postinjury individually caged with free access to food and water. On day 14, the mice were euthanized and the tissue surrounding the pressure ulcer wounds dissected and processed for subsequent histology. Paired H&E ($n=7$) and MT-stained ($n=7$) tissue sections from this model were included in the validation phase of the scoring system ($n=2$ healthy WT control, $n=5$ delayed healing).

Model 4. Burn wounds. A dorsal burn injury with concurrent Achilles tenotomy was induced on 6-week-old male C57BL/6 mice as previously described [13]. The mice were housed individually under standard conditions with free access to drinking water and food. Animals were treated $\times 3$ times per week with either Dasatinib or PBS vehicle control for a period of 9 weeks postinjury. The animals were euthanized, the skin peeled off the back, and a small sample processed for subsequent histology. H&E sections ($n=10$) from this model were included in the validation phase of the scoring system ($n=5$ control; $n=5$ treated).

Sample processing and image analysis

Tissue sections from models 1 to 3, were harvested (fixed in formalin), processed (embedded in paraffin and sectioned at 5 μm), deparaffinized (xylene immersion), and stained

(H&E, MT) using standardized histological procedures. Tissue sections from model 4 were harvested, cryopreserved (OCT), and sectioned at 10 μm before staining (H&E) using standardized histological procedures. The sample processing and staining was done at the time of harvest at each of the institutions. All images (tile scan using a light microscope with ×4 or ×10/0.25 objective) were retrospectively analyzed using Fiji Image J software (NIH.gov). Before taking any quantitative measurements the scale was set manually for each image based on the scale bar embedded at the time of acquisition.

Optimization of scoring system

For the initial phase of this study paired H&E ($n=10$) and MT ($n=10$) stained tissue sections derived from wild-type control mice with excisional wounds *(model 1)* were selected for analysis and optimization of the proposed scoring system. The selected tissue sections were all from day 7 postwounding but varied in quality and stage of healing. Sections that were difficult to interpret and/or contained processing artefacts were purposefully included in this initial analysis. These samples were analyzed for all the parameters indicated in Fig. 1 by $n=6$ independent investigators following a step-by-step preliminary standard operating procedure (SOP). The purpose of this initial phase of the study was to (1) optimize and clarify parameters in SOP to limit investigator bias and variability; (2) compare the consistency of parameters assessed using H&E *vs* MT staining.

Validation of scoring system

After optimization of the scoring system and the initial data analysis, a total of $n=54$ sections derived from the four different wound models were randomized and blinded. The optimized scoring system (Table 1) was validated with the blinded sections randomly assigned to two groups of independent investigators ($n=5$ per group) for analysis using the optimized step-by-step SOP. As part of the validation process, each investigator furthermore assigned a quality rating to each image using the following criteria: (1) – Poor quality due to staining; (2) – Poor quality due to processing artefacts; (3) – Good quality but difficult to interpret and identify wound area; (4) – Good quality; (5) – Excellent quality. If a sample was of very poor quality and affected the investigator's ability to take accurate measurements that sample was excluded from the validation process during the data Quality Control phase of this study. Each investigator also provided comments indicating challenges experienced when analyzing a specific sample. From the $n=54$ samples assessed, $n=5$ slides were excluded from analysis.

Statistical analysis

All statistical analysis was performed using GraphPad Prism (version 9.0.2). The threshold level of significance was defined at $P<0.05$. During the initial phase of the study, Spearman's correlation analysis was used to determine the correlation between the independent measures for each parameter from paired H&E and MT sections ($n=10$ paired slides; model 1). For the independent verification of the scoring system in the different models, quality control was performed on the blinded data for each sample to ensure that the investigators followed the guidelines set out in the SOP. Outliers were identified and flagged if one or two out of the five independent measures differed substantially from the other independent measures, and therefore placed the score in a different category. These outliers for each parameter were excluded to calculate a validated score for each sample (average of independent scores excluding outliers). The validated score was therefore calculated based on at least three corresponding independent measures for every single parameter. In the few cases that independent measures were slightly less consistent, the average of all five independent measures were used to calculate the validated score for that parameter. Using this validated score as the ''TRUE POSITIVE'' (TP) value and the outliers as the ''FALSE NEGATIVES'' (FN), the sensitivity for each parameter was calculated using the following formula: Sensitivity = [number of TP values/(number of TP values + number of FN values)] × 100 as previously described [14]. The mean ± SD of the overall histology scores for the independent investigators (without excluding outliers) and the number of independent scores that fall within 2 points of the validated score is reported.

Results

Validated histology score (All parameters)

Figure 1A and Table 1 provide an overview of the scoring system that was developed and validated in this study. The mean ± SD of the overall independent scores (including outliers) for each slide analyzed per model is presented in Fig. 1B–E. During the validation phase of the study 95% of the independent scores that assessed all 6 parameters per slide fell within 2 points (out of a maximum total of 12 points) of the validated score. Poor sample quality (artefact) or difficulty identifying the wounded area were evident in

FIG. 1. Histology score. **(A)** Visual overview of the histology scoring system illustrating the various phases of wound healing (1–4) from injury to either completely healed or scaring. The overlap of physiological processes that occur as part of healing, are indicated within each of the phases using a visual analog method. The approximate timeframe (days post wounding) that corresponds with each of the phases of healing is indicated at the *top* of the illustration. The timeframe is dependent on the type of wound and the animal model. The histology score is based on set criteria using various quantitative and semi-quantitative measures to assess each of the physiological parameters in either H&E or MT-stained sections (refer to Table 1). The parameters indicated by * cannot be accurately assessed using histology sections and require antibody-based cell-specific immunohistochemistry staining. **(B–E)** Histology score (mean ± SD) for the slides from each model analyzed by $n=5$ independent investigators in a randomized blinded fashion. H&E, Hematoxylin & Eosin; MT, Masson's Trichrome. Color images are available online.

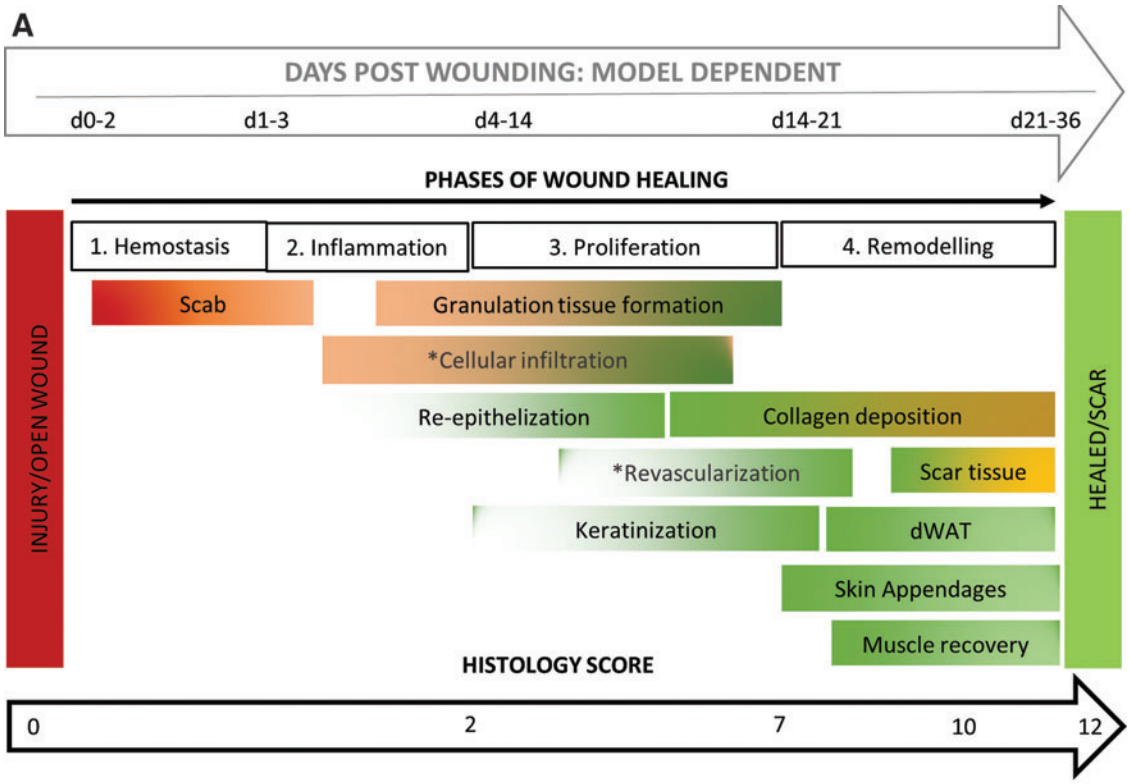
A
DAYS POST WOUNDING: MODEL DEPENDENT
d0-2
d1-3
d4-14
d14-21
d21-36
PHASES OF WOUND HEALING
1. Hemostasis
2. Inflammation
3. Proliferation
4. Remodelling
INJURY/OPEN WOUND
HEALED/SCAR
Scab
Granulation tissue formation
*Cellular infiltration
Re-epithelization
Collagen deposition
*Revascularization
Scar tissue
Keratinization
dWAT
Skin Appendages
Muscle recovery
HISTOLOGY SCORE
0
2
7
10
12

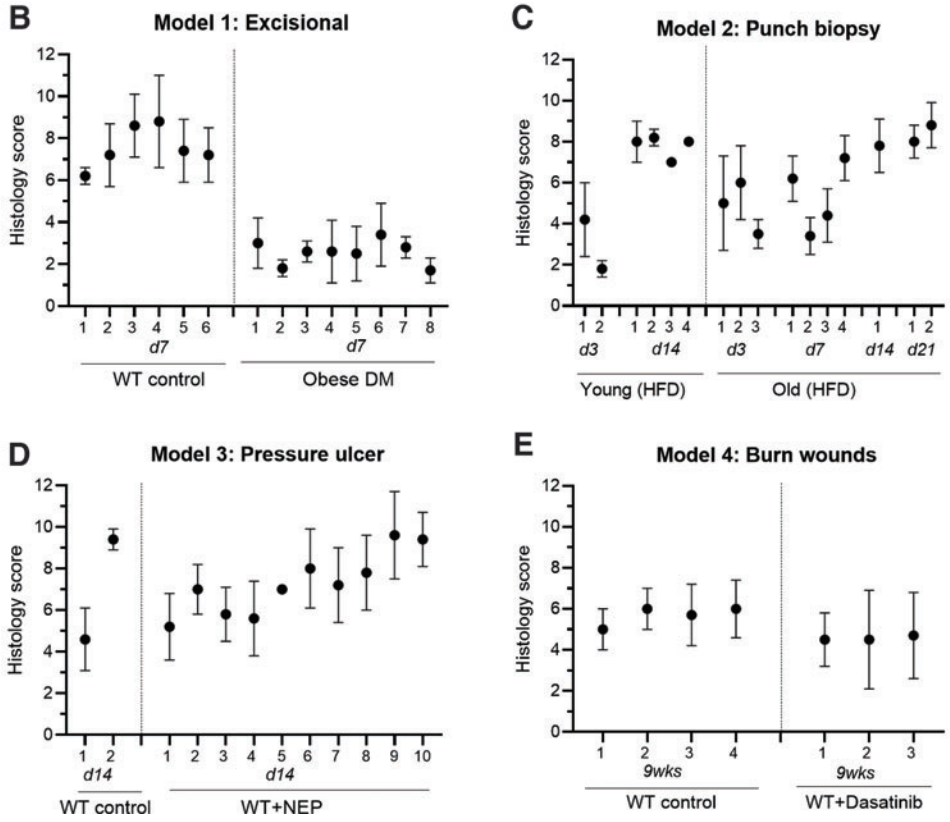
B
Model 1: Excisional
Histology score
d7
d7
WT control
Obese DM
C
Model 2: Punch biopsy
Histology score
d3
d14
d3
d7
d14
d21
Young (HFD)
Old (HFD)
D
Model 3: Pressure ulcer
Histology score
d14
d14
WT control
WT+NEP
E
Model 4: Burn wounds
Histology score
9wks
9wks
WT control
WT+Dasatinib

Table 1. Histology Scoring System: Description of Parameters

Parameter	*Description*	*Criteria*	*Score*	*Contribution*[3]	*Sensitivity*[4]
Re-epithelization[1]	Complete	95–100%	2	16.66%	92%
% = [distance of axis covered	Partial	<95%; >0%	1		
by epithelium (a) + (b)]/	None	0%	0		
[distance of minor axis between original wound edges (c)] × 100					
Epidermal thickness index[2]	Normal	95–105%	2	16.66%	89%
ETI = [average thickness of	Hypertrophy	>105%	1		
epidermis in wound area	Hypoplasia	<95%	0		
(P2)]/[average thickness of epidermis in uninjured skin (P1)] × 100					
Recommendation: only assess if Re-epithelization = complete					
Keratinization	Yes	Loosely attached/lost layers	2	16.66%	95%
Visual inspection		OR thick parakeratotic			
Recommendation:		stratum corneum			
only assess if re-epithelization = complete	No	None	0		
Granulation tissue	Intact dermis	Dermal layer intact no	2	16.66%	88%
Visual inspection and		granular infiltrates			
Absolute measure (μm)		consistent with healing			
	Thick GT	>100 μm	1		
	Thin GT	<100 μm	0		
Remodeling	Complete	All of the following	2	16.66%	82%
Visual inspection		parameters visible within wound area: (1) Dermal white adipose tissue; (2) Skin Appendages; (3) Panniculus carnosus regeneration			
	Partial	Either of the following parameters visible within wound area: (1) Collagen deposition; (2) Dermal white adipose tissue	1		
	None	No evidence of remodeling	0		
Scar elevation index[2]	Normal	95–105%	2	16.66%	82%
SEI = [average dermis	Hypertrophied	>105%	1		
thickness in wound area	Hypoplasia	<95%	0		
(P2)]/[average dermis thickness in uninjured skin (P1)] × 100					

For all quantitative parameters, measurements should be taken at five positions. To avoid investigator bias, sample analysis should be done blinded and randomized by five independent investigators.

[1](a) refers to distance from the one wound edge covered by epithelium; (b) refers to distance from the other wound edge covered by epithelium; (c) refers to the size of the original wound.

[2](P1) refers to uninjured skin; (P2) refers to wound area.

[3]Weighted contribution to the overall score.

[4]Sensitivity = [number of TP values/(number of TP values + number of FN values)] × 100.

FN, false negative; GT, granulation tissue; TP, true positive.

the investigators comments for the specific samples in which all 6 parameters was not assessed or where an independent score differed from the validated score by more than 2 points. No correlation was evident between the quality rating assigned to each sample and the deviation in independent scores, as investigators tended to assign a lower rating to sections with open wounds regardless of the staining/processing quality. Representative images illustrating the wound area in the different wound models are presented in Fig. 2.

Re-epithelization (Parameter 1)

The percentage re-epithelization (%) was used as a measure for wound closure (refer to Fig. 3A and Table 1 for an illustration on the exact method for assessing this parameter). The initial analysis during optimization indicated that re-epithelization can be accurately quantified in either H&E or MT-stained sections. When paired samples were analyzed independently the correlation between measurements taken in

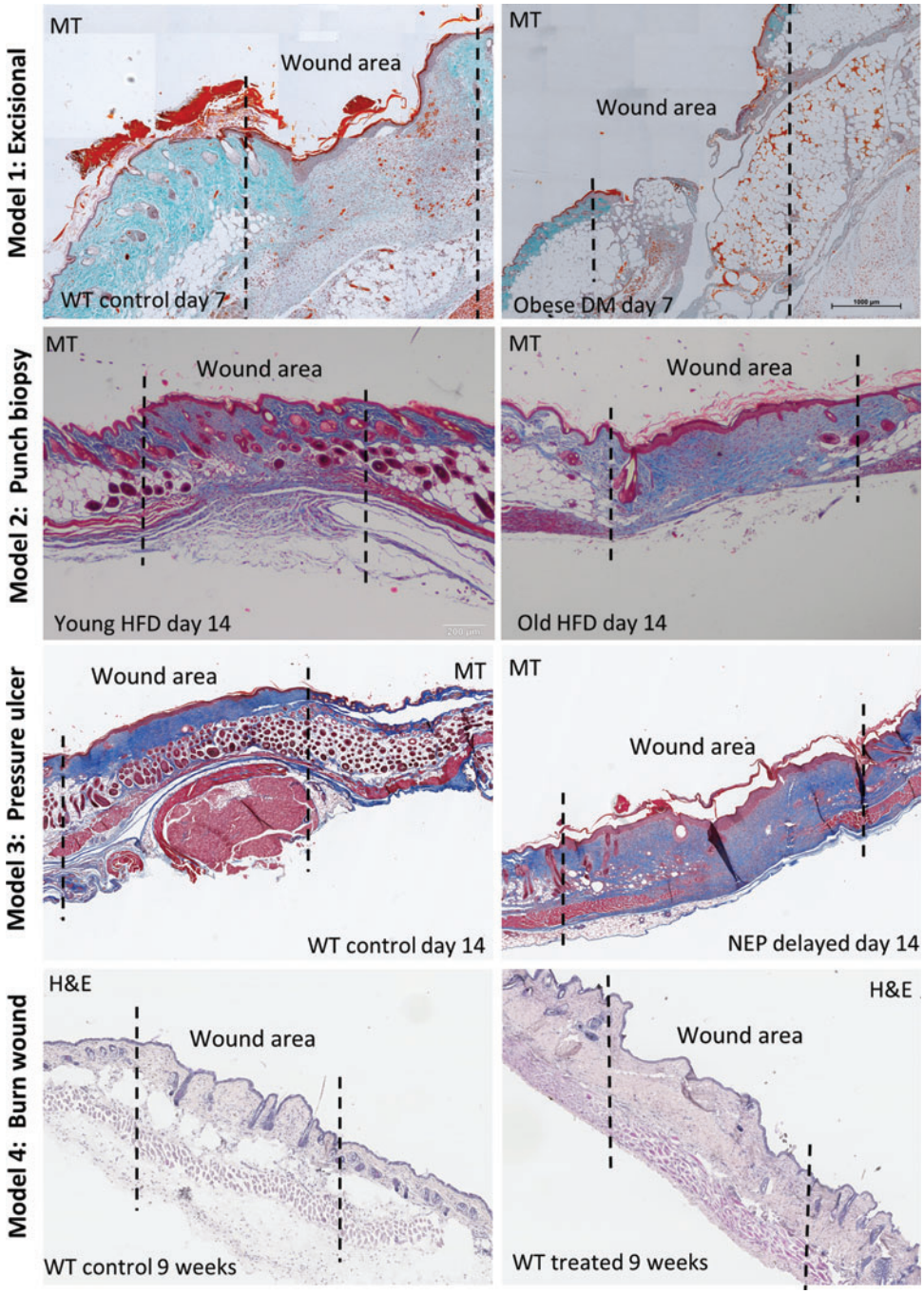

FIG. 2. Wound sections. Representative MT (model 1–3) and H&E (model 4) stained sections derived from each of the wound models. Model 1. WT control (C57BL/6J) and obese type 2 DM (B6.Cg-lep^{ob}/J, ob/ob) mice with excisional wounds 7 days postinjury. Model 2. Young and old wild-type control (C57BL/6J) mice on a HFD with punch biopsy wounds. For this model representative images of day 14 postinjury are presented although sections from days 3,7,14, and 21 postinjury were analyzed. Model 3. Wild-type control (C57BL/6J) mice with pressure ulcers 14 days postinjury. To delay healing, NEP was injected subcutaneously in the wound area in a subgroup of mice. Model 4. WT control (C57BL/6J) mice with burn wounds 9 weeks postinjury. A subgroup of mice was treated with Dasatinib. The wound area is indicated with *dotted lines*. HFD, high fat diet; WT, wild-type. Color images are available online.

H&E and MT-stained sections was $R^2 = 0.9321$ ($P < 0.0001$) ($n = 66$ data points) (Fig. 3B). Complete re-epithelization was evident when the newly formed epithelial tissue covered 95%–100% of the wounded area (score = 2), partial re-epithelization was defined as <95% of wounded area covered by epithelial tissue (score = 1) with epithelial tongues clearly visible. If there were no signs of re-epithelization and the wound remained completely open, no points were awarded for this parameter (score = 0). The overall sensitivity for this parameter was 92% (233 data points) during the validation phase of this study across all the wound models.

Epithelial thickness index (Parameter 2)

The epithelial thickness in the uninjured skin and wounded area was evaluated to calculate the epithelial thickness index (ETI) (refer to Fig. 3C and Table 1 for an illustration on the assessment method). The correlation between H&E and MT was $R^2 = 0.7155$ ($P < 0.0001$) ($n = 69$ data points) for the calculated ETI when paired samples were analyzed independently (Fig. 3D). Hypertrophy of the epidermis (ETI >105%) is prominent during re-epithelization and was evident in samples with both partial and complete re-epithelization. It is, however, recommended that ETI is only assessed in samples with

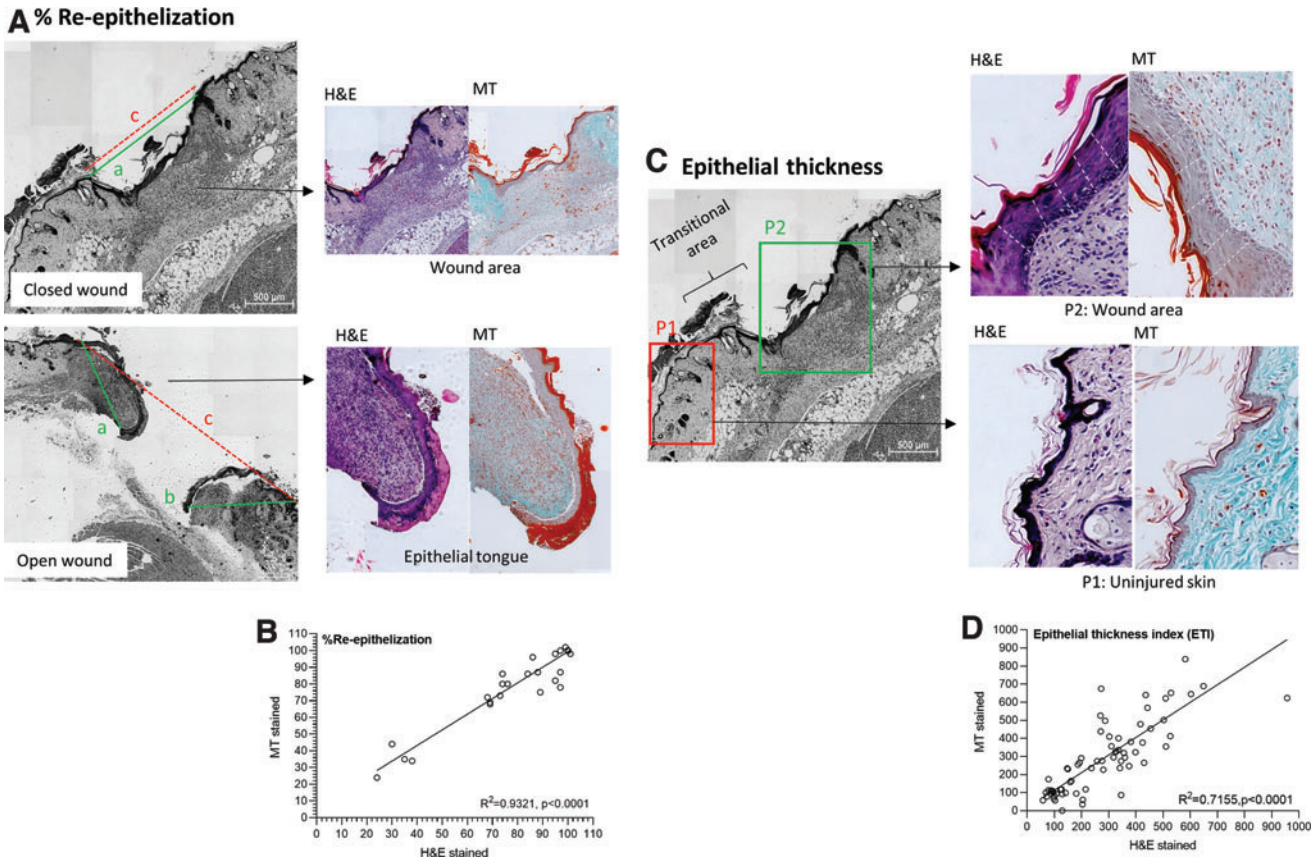

FIG. 3. Re-epithelization and epithelial thickness index. Representative histology sections with examples on **(A)** Assessing the distance of axis covered by new epithelium (a and b – *green line*) and the distance of the minor axis between the original wound edges (c – *red dotted line*), in either a closed wound or open wound. **(B)** Spearman's correlation comparing re-epithelization assessed in paired MT an H&E sections. **(C)** Assessing epithelial thickness in the wound area (P2) and uninjured healthy skin (P1) by taking five measures (*white dotted lines*) in each area. **(D)** Spearman's correlation comparing epithelial thickness index as assessed in paired MT an H&E sections. Color images are available online.

complete re-epithelization and that it is used as indicator of epithelial maturation in the wounded area. Although epidermal hypertrophy is indicative of healing, the epidermis has not yet returned to its uninjured (prewounded) state and only 1 point should thus be awarded (score = 1). A return to normal ETI (95%–105%) (score = 2) is often only observed in a completely healed wound after the final stages of remodeling. In the respective wound models, epithelial thickness in the uninjured skin was determined as follows: *Model 1*: 16.8 ± 10.4 μm (WT control); 28.4 ± 20.8 μm (obese DM); *Model 2*: 27.0 ± 23.2 μm (young); 28.6 ± 15.9 μm (old); *Model 3*: 27 ± 18.6 μm (WT control); *Model 4*: 14.1 ± 4.4 μm (WT control). Hypertrophy of the epidermis was prominent during healing with epithelial thickness increasing two to four-fold (*Model 1* WT control: ETI 325% ± 154%; *Model 2* young: ETI 227% ± 127%; *Model 2* old: ETI 346% ± 230%; *Model 3* WT control: ETI 351% ± 186%; *Model 4* WT control: ETI 90% ± 22%). During the validation phase of this study the sensitivity of ETI was 89% (133 data points) across all the wound models.

Keratinization (Parameter 3)

Keratinization is observed as loosely attached/lost layers of keratin or as a thick parakeratotic stratum corneum layer on the superficial surface above the epidermis. It can be assessed visually in either H&E or MT-stained sections (Fig. 4). During optimization of the scoring system the initial analysis indicated that it is difficult to define partial keratinization and that it was dependent on the investigator's subjective interpretation of a sample. This parameter was therefore adapted to be semi-quantitative and should be reported as either present (YES; score = 2) or absent (NO; score = 0) in the wounded area. This parameter can only be assessed accurately if re-epithelization is complete. In the cases where re-epithelization was complete, the sensitivity for assessing keratinization was 95% (133 data points) across all of the wound models.

Granulation tissue (Parameter 4)

The presence and/or absence of granulation tissue should be clearly defined. The lack of granulation tissue because the dermis is intact, and no granular infiltrates are evident due to healing and remodeling (score:2) should be distinguished from a lack of granulation tissue in a nonhealing wound (score:0) (Fig. 5A). Preliminary analysis indicated that the surface area or size of the granulation tissue is influenced by multiple confounding factors and should not be used as a scoring parameter. Instead, the thickness of granulation tissue (>100 μm; score = 1) provides a more

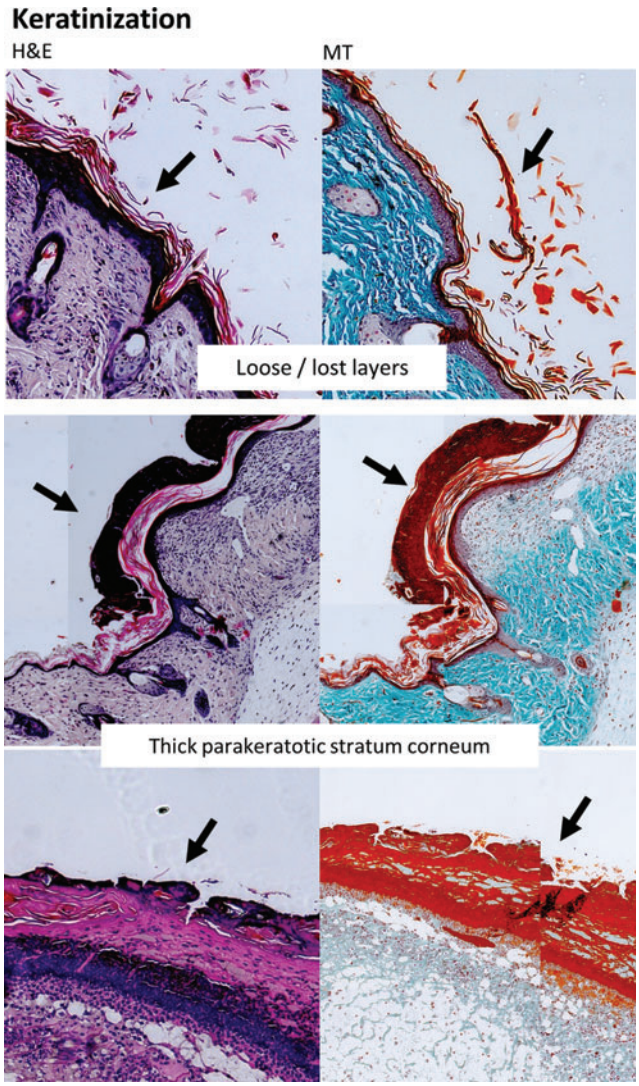

FIG. 4. Keratinization. Representative MT and H&E images illustrating the keratinization as either loose/lost keratin layers or as a thick parakeratotic stratum corneum (*black arrows*). Color images are available online.

accurate indication that healing is progressing into phase 3. The correlation between H&E and MT was $R^2 = 0.8549$ ($P < 0.001$) for granulation tissue thickness ($n = 68$ data points) when paired samples were analyzed independently (Fig. 5B). In the respective wound models, granulation tissue thickness was as follows: *Model 1:* 452 ± 406 μm (WT control day 7); 77 ± 179 μm (obese DM day 7); *Model 2:* 143 ± 156 μm (young day 3); 145 ± 186 μm (young day 14); 275 ± 126 μm (old day 3); 293 ± 212 μm (old day 7); 291 ± 53 μm (old day 14); 108 ± 117 μm (old day 21); *Model 3*: 475 ± 471 μm (WT control day 14); 658 ± 620 μm (WT+NEP day 14); *Model 4:* 75 ± 128 μm (WT control); 91 ± 142 μm (WT+treatment). Refer to Fig. 5A for an illustration on how to measure granulation tissue thickness. The overall sensitivity for this parameter was 88% (176 data points).

Optional parameters to assess if granulation tissue is present include cellular infiltration and revascularization. The initial analysis during the optimization phase of this study demonstrated that it is not possible to accurately assess these parameters in histology sections without the use of antibody-specific staining. Two methods were compared to assess cellular infiltration in histology sections: the percentage surface area (%) representing cellular nuclei and manual counting of the number of cells/mm^2 within granulation tissue. Of these two methods, the use of a threshold tool to determine % surface area proved to be the most consistent based on independent analysis; however, results did vary between H&E and MT-stained sections and false positive results were observed if capillaries or skin appendages were evident within the granulation tissue (data not shown). Examples of cell-specific markers that can be used to assess cellular infiltration using antibody based IHC staining are provided in Fig. 5C. The accurate identification of capillaries is also not possible in histology slides. While Fig. 5D indicates the presence of capillaries with red blood cells visible in the lumen, it also displays similar round structures that could be either adipose tissue, capillaries, or random holes due to fixation artifacts. The use of antibody-based staining is thus required to ensure accurate distinction among these structures.

Scar elevation index (Parameter 5)

This parameter is an indirect assessment of scar formation based on the presence of a hypertrophied dermis in the wound area. Refer to Fig. 6A for an illustration of the layers evident in a full-thickness skin section starting with epidermis, then dermis spanning from the subepithelial layer to the *panniculus carnosus* muscle proximal and subcutaneous white adipose tissue. If the dermis in the wounded area is intact and its thickness is consistent with that of uninjured skin, the wound is likely in the final stages of healing (score:2). Excessive collagen deposition as is evident in scar tissue formation, would, however, result in hypertrophy of the dermis (score:1), whereas an underdeveloped dermis indicates that healing is still in the early stages (score:0) (Fig. 6B). The correlation between H&E and MT-stained sections for assessing the scar elevation index (SEI) was $R^2 = 0.9113$ ($P < 0.0001$) ($n = 60$ data points) with independent analysis during the optimization phase of this study (Fig. 6C). In the respective wound models, dermal thickness in the uninjured skin was as follows: *Model 1:* 975 ± 524 μm (WT control); 1173 ± 739 μm (obese DM); *Model 2:* 453 ± 240 μm (young); 589 ± 249 μm (old); *Model 3:* 796 ± 318 μm (WT control); *Model 4:* 366 ± 331 μm (WT control). The overall sensitivity of this parameter was 82% (225 data points).

Remodeling (Parameter 6)

Remodeling should ideally be assessed in MT-stained tissue sections, since collagen deposition cannot be observed with H&E staining. H&E sections will therefore have a disadvantage with an overall score that is 1 point lower than its MT-stained counterpart, in cases where remodeling is evident. This parameter is semi-quantitative and based on visual inspection of the wound area. Signs of remodeling include the presence of dermal white adipose tissue (dWAT), skin appendages (hair follicles, sebaceous glands), and/or collagen deposition. During the early stages of remodeling there is some evidence of collagen deposition

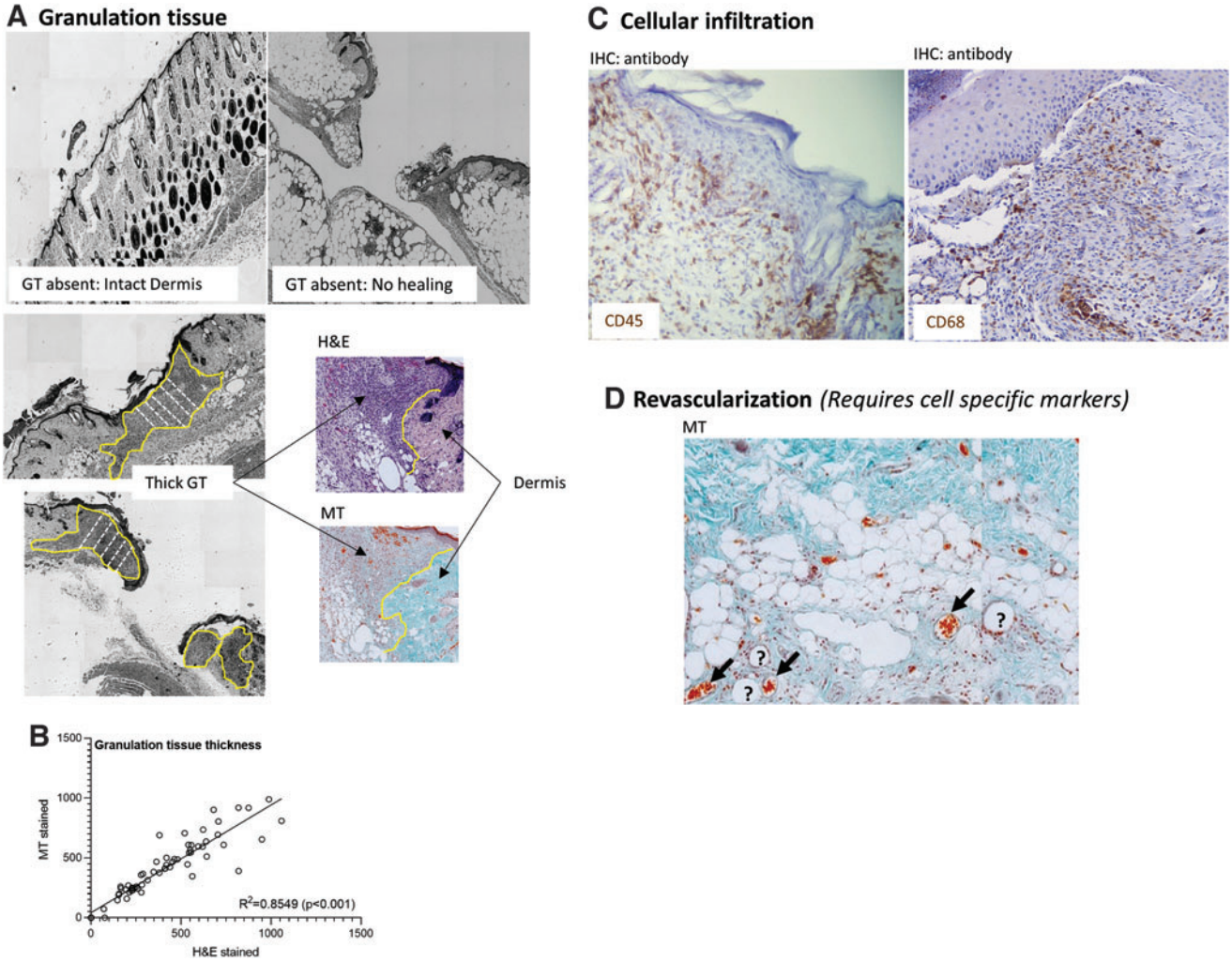

FIG. 5. GT. **(A)** Representative histology sections illustrating the difference between absent GT due to an intact dermis associated with complete healing and remodeling and the absence of GT due to a lack of healing. The assessment of GT (area indicated in *yellow*) thickness in a closed and open wound by taking five measures (*white dotted lines*) is illustrated. **(B)** Spearman's correlation comparing granulation tissue thickness assessed in paired MT an H&E sections. **(C)** Representative IHC images illustrating antibody-based staining (*brown*) [CD45 leukocyte (monoclonal CD45 antibodies; BD Biosciences) and CD68 macrophage (rabbit polyclonal; Abcam)] to identify specific cellular infiltrates in GT. **(D)** Representative MT-stained section illustrating capillaries with red blood cells present within lumen (*black arrows*) and similar unidentified structures (*question marks*) emphasizing the importance for cell-specific antibody based IHC to assess revascularization in GT. GT, granulation tissue; IHC, immunohistochemistry. Color images are available online.

and/or dWAT with no or very little skin appendages present in the wound area (score:1) (Fig. 6D). Remodeling is considered complete or in the final stages when a multitude of skin appendages are present in the wound area and when the *panniculus carnosus* muscle is intact (score:2) (Fig. 6D). The overall sensitivity for this parameter was 82% (235 data points) across all wound models.

Discussion

The need for accurate histological grading of wounds based on the different parameters within each phase of wound healing has been emphasized in reviews of the skin wound healing literature [15–17]. Despite numerous tools available for the clinical evaluation of wounds in human patients [6,18], to our knowledge this is the first study to statistically standardize and validate a histopathologic scoring system for grading murine skin wounds. The scoring system was based on parameters routinely assessed in literature and was selected to correspond with the different phases of healing. The image quantification methods implemented in this scoring system were selected based on accessibility, with regards to both the ease of interpretation and availability of software. The histological assessment method for these parameters was refined and simplified to ensure reproducibility before the scoring system was validated in four different wound models. The scoring system was designed in such a way that the lowest score (score:0) is associated with an open/unhealed wound as is evident immediately and within the first day postinjury, whereas the highest score (score:12) is associated with a completely closed and healed wound without excessive scarring. The

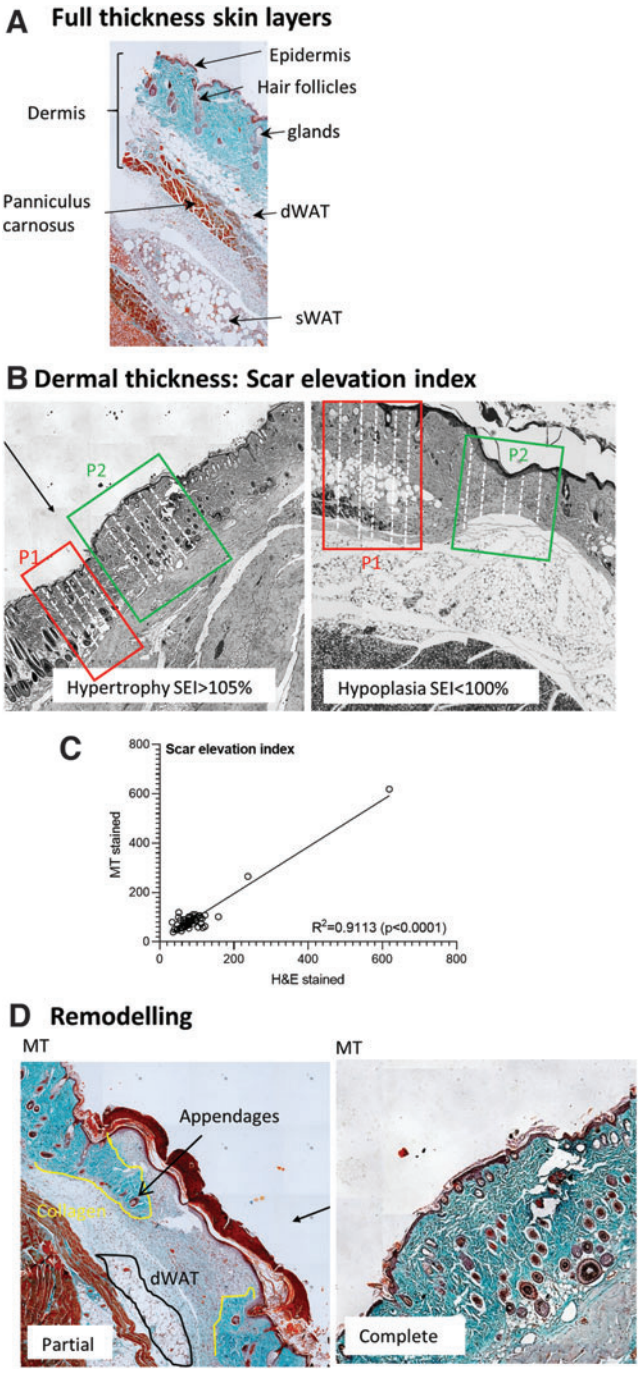

FIG. 6. Scarring and remodeling. **(A)** Representative MT image illustrating the full-thickness skin layers in healthy uninjured mouse skin. **(B)** Assessing dermal thickness in uninjured skin (P1) and the wound area (P2) by taking five measures (*white dotted lines*) to determine the SEI. Dermal hypertrophy is associated with scar formation and hypoplasia with a wound that is still in the earlier stages of healing. **(C)** Spearman's correlation comparing the SEI (dermal thickness) assessed in paired MT an H&E sections. **(D)** Representative MT images illustrating the signs of partial and complete remodeling based on the presence of collagen deposition, dWAT and skin appendages in the wound area. SEI, scar elevation index. Color images are available online.

overall histology score in this study therefore corresponds with the stage of healing. Nevertheless, the time frame of healing is dependent on the wound etiology and differs between models. It is thus essential that appropriate wild-type and untreated control groups are included in all studies for comparison purposes. Although murine models are commonly used to study wound healing, it is not a perfect representation of human skin and it therefore does not always predict clinical outcome [19,20]. It is thus essential that observations from murine models are interpreted accurately.

In human skin, wounds close through granulation tissue formation whereas wound contraction mediated by the *panniculus carnosus* muscle occurs in mice before the formation of granulation tissue [19]. The percentage wound closure as evident on a macroscopic level is a widely used measure to indicate either accelerated or delayed healing responses in murine models [21–24]. Furthermore, there are several limitations associated with the use of images to quantify macroscopic wound closure, especially since non-perpendicular images (the distance and angle where the camera and the reference ruler is positioned) can significantly underestimate surface area [15]. Wound contraction (% wound closure) is furthermore not representative of wound bed preparation and is not ideal to use in translational studies. Re-epithelization is therefore a more appropriate measure to assess wound closure. When assessing the epithelial thickness, care should be taken to ensure that the epithelial tongue (newly formed epithelium), transitional epidermis (inflamed/edema area adjacent to the wound), and uninjured skin (not affected by healing response) [25] are accurately identified. This is especially important when open wounds are analyzed, since the thicker epithelium evident in the transitional epidermis should not be mistakenly reported as epithelial thickness in the wounded area, to avoid false positive scores. It is therefore recommended that ETI is only assessed in wounds with complete re-epithelization and that it is used as an indicator of epidermal maturation.

During the proliferation stage of healing, keratinocyte migration plays a crucial role in re-epithelization and the formation of granulation tissue by interacting with epithelial cells, dermal fibroblasts, and other granular infiltrates through cell–cell contact and paracrine secretion [26,27]. Formation of the stratum corneum is therefore evident before complete wound closure and re-epithelization. This process is complex and partial keratinization cannot be accurately quantified in histology sections. During terminal differentiation of epidermal keratinocytes, the formation of keratin polypeptides and their polymerization into intermediate filaments and bundles occur, which can be visualized in histology sections [28]. The presence of loosely attached keratinized layers or thicker stratum corneum after complete re-epithelization has occurred and can therefore be interpreted as signs of terminal differentiation and the progression of healing.

Similarly, the formation of granulation tissue is complex and involves the interplay of numerous cell types such as keratinocytes, epithelial cells, fibroblasts, and inflammatory/immune cells within the wound area. It is characterized histologically by the presence of a large number of cellular nuclei within the extracellular matrix [29]. Granulation tissue usually forms at the base of the wound edges to replace necrotic tissue with new tissue and vasculature, with it being

at its thickest during the proliferation stage of healing and then being slowly replaced by collagen and/or scar tissue during the remodeling stages of healing [29]. The size (surface area) of granulation tissue is influenced by numerous confounding factors such as wound type (method of injury), size and depth of the original wound, tissue harvesting, and processing artefacts and is therefore difficult to standardize as a measurement across models. Thickness of granulation tissue is a more accurate parameter to use as part of the histology scoring system and has been reported in the literature [30].

In wounds that are transitioning from the proliferative to remodeling phases of healing, the focus is on restoration of skin integrity. During remodeling, collagen deposition and maturation, dWAT and skin appendages becomes evident within in the wounded area. In full-thickness wounds, regeneration of the *panniculus carnosus* muscle is also evident toward the end of this stage. Remodeling is known to occur for an extended period of time after macroscopic wound closure, and is an essential process to restore tissue function [31]. The characteristics of the animal model should be considered when visual inspection is performed to identify signs of remodeling. In obese or extremely lean mice (young or otherwise), the presence or absence of dWAT for example can be wrongly interpreted as either a sign of partial remodeling or the lack of complete remodeling. This parameter is therefore more descriptive and dependent on the investigators experience and understanding of the murine model. The healthy noninjured skin adjacent to the wound area should be used as guide when a remodeling score is assigned and should be kept consistent between samples. The outcome of remodeling is a completely healed wound with either restored tissue integrity and function or scar formation. Excessive collagen deposition during the remodeling phase leads to scar formation and hypertrophy of the dermis. The SEI, which is based on the dermal thickness in the wound area compared to uninjured healthy skin is a relatively simple parameter to indicate whether excessive scarring has occurred. This is sufficient as a parameter in an overall histological scoring system and has been reported in the literature [32–35]. More detailed analysis that include collagen fiber orientation and/or skin elasticity is, however, required for investigations focused specifically on collagenous scarring and its characteristics [36].

Conclusion

This histological scoring system defines and describes the minimum recommended criteria for assessing wound healing dynamics. The experience and ability of investigators to accurately identify structures in histology slides at different stages of healing is crucial for consistency and repeatability of measures to deliver meaningful results. It should also be noted that sampling, sectioning, staining, and imaging of tissues can greatly influence the consistency of histological data. It is recommended that all sections be analyzed in a randomized blinded fashion by at least three independent investigators and great care should be taken not to introduce unintentional bias. Depending on the aim/objective of a specific study the scoring system should be complemented by immunohistochemistry (IHC) and more in-depth analysis of underlying cellular and molecular mechanisms.

Author Disclosure Statement

Emma Rogers, Katie Hamel, Trivia Frazier, and Jeff Gimble are employees of Obatala Sciences. Trivia Frazier and Jeff Gimble are co-founders and co-owners of Obatala Sciences. Jeff Gimble is also a co-founder and co-owner of Talaria Antibodies.

Funding Information

Funding for Dr B. Levi included the following: DOD W81XWH-17-MBRP-CTA (MB170041).* Funding for Dr M van de Vyver included the National Research Foundation (NRF) and South African Medical Research Council Self-initiated research grant.

References

1. Martinengo L, M Olsson, R Bajpai, M Soljak, Z Upton, A Schmidtchen, J Car and K Järbrink. (2019). Prevalence of chronic wounds in the general population: systematic review and meta-analysis of observational studies. Ann Epidemiol 29:8–15.
2. Frykberg RG and J Banks. (2015). Challenges in the treatment of chronic wounds. Adv Wound Care (New Rochelle) 4:560–582.
3. Nussbaum SR, MJ Carter, CE Fife, J DaVanzo, R Haught, M Nusgart and D Cartwright. (2018). An economic evaluation of the impact, cost, and medicare policy implications of chronic nonhealing wounds. Value Health 21:27–32.
4. Mulder GD, DK Lee and NS Jeppesen. (2012). Comprehensive review of the clinical application of autologous mesenchymal stem cells in the treatment of chronic wounds and diabetic bone healing. Int Wound J 9:595–600.
5. Sen CK. (2019). Human wounds and its burden: an updated compendium of estimates. Adv Wound Care (New Rochelle) 8:39–48.
6. Klassen AF, ELWG van Haren, TC van Alphen, S Cano, KM Cross, A-M van Dishoeck, KL Fan, M Michael Hoogbergen, D Orgill, et al. (2021). International study to develop the WOUND-Q patient-reported outcome measure for all types of chronic wounds. Int Wound J [Epub ahead of print]; DOI: 10.1111/iwj.13549
7. Wang P-H, B-S Huang, H-C Horng, C-C Yeh and Y-J Chen. (2018). Wound healing. J Chin Med Assoc 81:94–101.
8. Boodhoo K, M Vlok, DL Tabb, KH Myburgh and M van de Vyver. (2021). Dysregulated healing responses in diabetic wounds occur in the early stages postinjury. J Mol Endocrinol 66:141–155.
9. Čoma M, L Fröhlichová, L Urban, R Zajíček, T Urban, P Szabo, Š Novák, V Fetissov, B Dvořánková, K Smetana and P Gál. (2021). Molecular changes underlying hypertrophic scarring following burns involve specific deregulations at all wound healing stages (Inflammation, Proliferation and Maturation). Int J Mol Sci 22:897.
10. Siddiqui AR and JM Bernstein. (2010). Chronic wound infection: facts and controversies. Clin Dermatol 28:519–526.
11. Kopcewicz M, K Walendzik, J Bukowska, A Kur-Piotrowska, S Machcinska, JM Gimble and B Gawronska-Kozak. (2020). Cutaneous wound healing in aged, high fat

*__Correction added__ on August 19, 2021 after first online publication of July 14, 2021: In the Funding information section the text ''NIH funding R61AR078072 and R01AR071379'' has been removed.

diet-induced obese female or male C57BL/6 mice. Aging (Albany NY) 12:7066–7111.
12. Strong AL, AC Bowles, CP MacCrimmon, SJ Lee, TP Frazier, AJ Katz, B Gawronska-Kozak, BA Bunnell and JM Gimble. (2015). Characterization of a murine pressure ulcer model to assess efficacy of adipose-derived stromal cells. Plast Reconstr Surg Glob Open 3:e334.
13. Thorpe CR, S Ucer Ozgurel, LC Simko, R Goldstein, GG Grant, C Pagani, C Hwang, K Vasquez, M Sorkin, et al. (2019). Investigation into possible association of oxandrolone and heterotopic ossification following burn injury. J Burn Care Res 40:398–405.
14. Trevethan R. (2017). Sensitivity, specificity, and predictive values: foundations, pliabilities, and pitfalls in research and practice. Front Public Health 5:307.
15. Masson-Meyers DS, TAM Andrade, GF Caetano, FR Guimaraes, MN Leite, SN Leite and MAC Frade. (2020). Experimental models and methods for cutaneous wound healing assessment. Int J Exp Pathol 101:21–37.
16. Gupta A and P Kumar. (2015). Assessment of the histological state of the healing wound. Plast Aesthet Res 2:239.
17. Gibson-Corley KN, AK Olivier and DK Meyerholz. (2013). Principles for valid histopathologic scoring in research. Vet Pathol 50:1007–1015.
18. Cullell-Dalmau M, M Otero-Viñas, M Ferrer-Solà, H Sureda-Vidal and C Manzo. (2021). A toolkit for the quantitative evaluation of chronic wounds evolution for early detection of non-healing wounds. J Tissue Viability 30:161–167.
19. Zomer HD and AG Trentin. (2018). Skin wound healing in humans and mice: challenges in translational research. J Dermatol Sci 90:3–12.
20. Gawronska-Kozak B, A Grabowska, M Kopcewicz and A Kur. (2014). Animal models of skin regeneration. Reprod Biol 14:61–67.
21. Mapoung S, S Umsumarng, W Semmarath, P Arjsri, P Thippraphan, S Yodkeeree and P Limtrakul Dejkriengkraikul. (2021). Skin Wound-Healing Potential of Polysaccharides from Medicinal Mushroom Auricularia auricula-judae (Bull.). J Fungi (Basel) 7:247.
22. Kang HJ, S Kumar, A D'Elia, B Dash, V Nanda, HC Hsia, ML Yarmush and F Berthiaume. (2021). Self-assembled elastin-like polypeptide fusion protein coacervates as competitive inhibitors of advanced glycation end-products enhance diabetic wound healing. J Control Release 333:176–187.
23. Moreira CF, P Cassini-Vieira, MCC Canesso, M Felipetto, H Ranfley, MM Teixeira, JR Nicoli, FS Martins and LS Barcelos. (2021). Lactobacillus rhamnosus CGMCC 1.3724 (LPR) improves skin wound healing and reduces scar formation in mice. Probiotics Antimicrob Proteins 13:709–719.
24. Wang Z, Y Wang, N Bradbury, C Gonzales Bravo, B Schnabl and A Di Nardo. (2020). Skin wound closure delay in metabolic syndrome correlates with SCF deficiency in keratinocytes. Sci Rep 10:21732.
25. Noguchi F, T Nakajima, S Inui, JK Reddy and S Itami. (2014). Alteration of skin wound healing in keratinocyte-specific mediator complex subunit 1 null mice. PLoS One 9:e102271.
26. Shetty S and S Gokul. (2012). Keratinization and its disorders. Oman Med J 27:348–357.
27. Werner S, T Krieg and H Smola. (2007). Keratinocyte-fibroblast interactions in wound healing. J Invest Dermatol 127:998–1008.
28. Deo PN and R Deshmukh. (2018). Pathophysiology of keratinization. J Oral Maxillofac Pathol 22:86–91.
29. Alhajj M, P Bansal and A Goyal. (2020). Physiology, Granulation Tissue. In: *StatPearls* [Internet]. StatPearls Publishing, Treasure Island, FL.
30. Galeano M, V Torre, B Deodato, GM Campo, M Colonna, A Sturiale, F Squadrito, V Cavallari, D Cucinotta, M Buemi and D Altavilla. (2001). Raxofelast, a hydrophilic vitamin E-like antioxidant, stimulates wound healing in genetically diabetic mice. Surgery 129:467–477.
31. Cañedo-Dorantes L and M Cañedo-Ayala. (2019). Skin acute wound healing: a comprehensive review. Int J Inflam 2019:3706315.
32. Jiang Z, L Zhao, F He, H Tan, Y Li, Y Tang, X Duan and Y Li. (2021). Palmatine-loaded electrospun poly(ε-caprolactone)/gelatin nanofibrous scaffolds accelerate wound healing and inhibit hypertrophic scar formation in a rabbit ear model. J Biomater Appl 35:869–886.
33. Feng Y, J-J Wu, Z-L Sun, S-Y Liu, M-L Zou, Z-D Yuan, S Yu, G-Z Lv and F-L Yuan. (2020). Targeted apoptosis of myofibroblasts by elesclomol inhibits hypertrophic scar formation. EBioMedicine 54:102715.
34. Ma L, LY Li and TL Zhao. (2020). Anti-inflammatory effects of ginsenoside Rg3 on the hypertrophic scar formation via the NF-κB/IκB signaling pathway in rabbit ears. Pharmazie 75:102–106.
35. Qian L-W, AB Fourcaudot, K Yamane, T You, RK Chan and KP Leung. (2016). Exacerbated and prolonged inflammation impairs wound healing and increases scarring. Wound Repair Regen 24:26–34.
36. Bailey AJ, S Bazin, TJ Sims, M Le Lous, C Nicoletis and A Delaunay. (1975). Characterization of the collagen of human hypertrophic and normal scars. Biochim Biophys Acta 405:412–421.

Address correspondence to:
Mari van de Vyver, PhD
Division of Clinical Pharmacology
Department of Medicine
Faculty of Medicine and Health Sciences
Stellenbosch University
Cape Town 7500
South Africa

E-mail: vandevyverm@sun.ac.za

Received for publication June 1, 2021
Accepted June 15, 2021
Prepublished on Liebert Instant Online June 15, 2021